JACS
JOURNAL OF THE AMERICAN CHEMICAL SOCIETY

ARTICLE

pubs.acs.org/JACS

# Structural Basis of Regiospecificity of a Mononuclear Iron Enzyme in Antibiotic Fosfomycin Biosynthesis

Danny Yun,[‡] Mishtu Dey,[†,‡] Luke J. Higgins,[‡,⊥] Feng Yan,[∥] Hung-wen Liu,[∥] and Catherine L. Drennan*[,†,‡,§]

[†]Howard Hughes Medical Institute, [‡]Department of Chemistry, and [§]Department of Biology, Massachusetts Institute of Technology, Cambridge, Massachusetts 02139, United States

[∥]Division of Medicinal Chemistry, College of Pharmacy, and Department of Chemistry and Biochemistry, University of Texas at Austin, Austin, Texas 78712, United States

Supporting Information

**ABSTRACT:** Hydroxypropylphosphonic acid epoxidase (HppE) is an unusual mononuclear iron enzyme that uses dioxygen to catalyze the oxidative epoxidation of (*S*)-2-hydroxypropylphosphonic acid (*S*-HPP) in the biosynthesis of the antibiotic fosfomycin. Additionally, the enzyme converts the *R*-enantiomer of the substrate (*R*-HPP) to 2-oxo-propylphosphonic acid. To probe the mechanism of HppE regiospecificity, we determined three X-ray structures: *R*-HPP with inert cobalt-containing enzyme (Co(II)−HppE) at 2.1 Å resolution; *R*-HPP with active iron-containing enzyme (Fe(II)−HppE) at 3.0 Å resolution; and *S*-HPP−Fe(II)−HppE in complex with dioxygen mimic NO at 2.9 Å resolution. These structures, along with previously determined structures of *S*-HPP−HppE, identify the dioxygen binding site on iron and elegantly illustrate how HppE is able to recognize both substrate enantiomers to catalyze two completely distinct reactions.

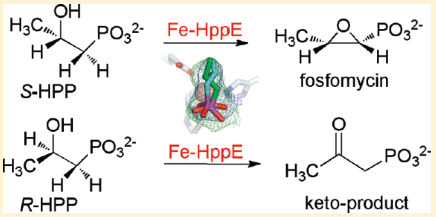


## INTRODUCTION

Fosfomycin, or (1*R*,2*S*)-1,2-epoxypropyl-phosphonic acid, is an antibiotic used in the treatment of lower urinary tract infections[1] and is effective against methicillin-resistant[2] and vancomycin-resistant[3] strains of *Staphylococcus aureus*. It targets the first committed step in cell wall biosynthesis by inhibiting the enzyme UDP-GlcNAc-3-*O*-enolpyruvyltransferase (MurA).[4,5] Key to the reactivity of fosfomycin is the epoxide ring in its scaffold. While epoxide rings are found in many natural products, the way in which the fosfomycin epoxide ring is biosynthesized by microbes such as *Streptomyces wedmorensis* and *Pseudomonas syringae* may be unique.[6,7] Unlike other characterized epoxidases that form epoxides through oxygen atom insertion, hydroxypropylphosphonic acid epoxidase (HppE) forms fosfomycin by catalyzing an oxidative cyclization reaction with retention of the substrate hydroxyl oxygen atom[8−10] (Scheme 1a). Despite one report[11] that HppE has some catalytic activity with zinc, recent studies show that under defined conditions, Zn−HppE does not produce fosfomycin, reaffirming this enzyme as a member of the mononuclear nonheme iron superfamily.[12]

HppE shares several features with other members of this superfamily, including the use of the so-called 2-His-1-carboxylate facial triad [$His_2$(Glu/Asp)] to coordinate an iron atom within a conserved $\beta$-barrel fold also known as a cupin fold.[9,10,13−15] With highest structural similarity to the mononuclear iron enzyme hydroxyethylphosphonate dioxygenase,[16] HppE is an unusual tetramer with four $\beta$-barrels intertwined with four α-helical domains, creating four active sites at each of the α−$\beta$ interfaces (Figure 1).[15] The substrate (*S*)-2-hydroxypropylphosphonic acid (*S*-HPP) binds directly to the iron center in these active sites, triggering conformational changes in the $\beta$-hairpin, or cantilever hairpin, which is directly above each facial triad.[15] While other mononuclear iron enzymes can undergo conformational changes when substrates bind,[17−19] the use of these $\beta$-strands is unique to HppE. This conformational change buries the hydrophobic portion of the substrate, reducing solvent accessibility of the active site and thus protecting high-energy iron−oxygen intermediates, such as a superoxide intermediate (Fe−$O_2^{\bullet-}$),[20] which may form during catalysis. For complete turnover, HppE also requires two exogenous electrons, and unlike many members of this superfamily, α-ketoglutarate does not serve this function. Instead, these electrons are derived from NAD(P)H and shuttled to the active site by a reductase in vivo.[6,9]

Another fascinating feature of HppE is that it recognizes both *S*-HPP and its enantiomeric substrate *R*-HPP and is an efficient catalyst with respect to both reactions.[21,22] Interestingly, *R*-HPP is not converted to an epoxide. Rather, this stereoisomer exclusively yields a ketone product, 2-oxopropylphosphonic acid (Scheme 1b).[21,22] To probe the mechanism of regiospecificity of HppE catalysis, both enantiomers of the substrate were synthesized incorporating fluorines in place of the C1 methylene hydrogens (*S*-FHPP and *R*-FHPP).[22] *S*-FHPP is a strong competitive inhibitor of HppE activity, while *R*-FHPP is a substrate and is converted to 1-difluoro-2-oxopropylphosphonic acid (Scheme 1c,d).[22] This result suggests that the reaction path is determined by the regiospecificity of hydrogen atom abstraction; a C1 hydrogen atom is abstracted from the *S*-HPP substrate, and a C2 hydrogen atom is abstracted from *R*-HPP. A radical

**Received:** March 21, 2011
**Published:** June 17, 2011





dx.doi.org/10.1021/ja2025728 | *J. Am. Chem. Soc.* 2011, 133, 11262–11269

**Scheme 1. HppE-Catalyzed Conversion of (a) *S*-HPP, (b) *R*-HPP, (c) *S*-FHPP, and (d) *R*-FHPP**

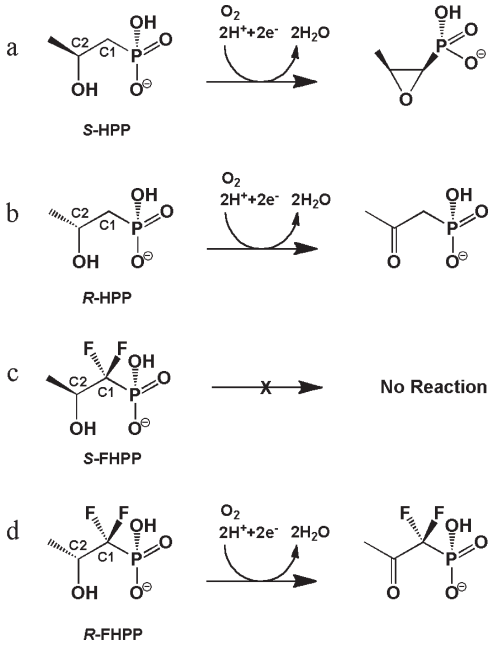


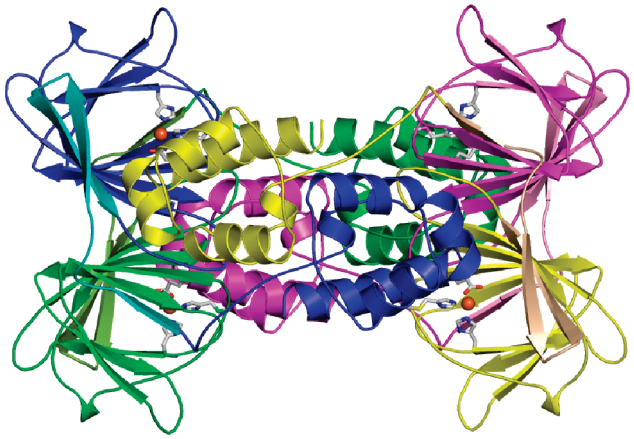

**Figure 1.** The HppE tetramer is shown colored by molecule in blue, magenta, yellow, and green, with strand 1 and the cantilever hairpin colored separately in cyan, pink, wheat, and limon, respectively. Iron atoms are shown as spheres (rust), and iron ligands are in sticks: carbon (gray), nitrogen (blue), oxygen (red).

centered at C1 would then yield the epoxide product, whereas the C2 radical yields the ketone.[22]

Although the results from these fluorinated analogues provide an explanation for why a different product is formed from each stereoisomer, we sought to understand why the enzyme would abstract a different hydrogen atom in each case. First, it is important to identify where dioxygen binds to the iron in the enzyme active site. While it has been proposed that dioxygen binds iron at the only open coordination site that exists when *S*-HPP is bound in the bidentate conformation,[15] here we use NO as a dioxygen mimic to obtain experimental evidence for this binding site. The next question is whether the *R*- and *S*-stereoisomers bind the iron active site in a different fashion, and, if so, what is the cause of differential binding? If they bind in the same fashion, can differences in C−H bond dissociation energies (calculated to be 96.5 and 89.0 kcal $mol^{-1}$ for *S*-HPP (C1−H) and *R*-HPP (C2−H), respectively[6]) explain the observed regiospecificity? To address these questions, we have solved a structure at 2.1 Å resolution of Co(II)−HppE with the *R*-stereoisomer of substrate bound. Additionally, we have determined the structure of the substrate enantiomer in complex with Fe(II)−HppE at 3.0 Å resolution. These structures reveal that *R*-HPP has a binding mode similar to that of *S*-HPP but differs with respect to the relative orientation of the C1, C2, and C3 positions. Furthermore, the structures illustrate that hydrogen atom accessibility to the proposed iron-superoxo intermediate species is sufficient to explain the regiospecificity of the HppE-catalyzed reactions.

## MATERIALS AND METHODS

**Materials.** *R*-HPP and *S*-HPP were synthesized as previously described.[9,10] Cobalt(II) chloride was purchased from Hampton Research (Aliso Viejo, CA), diethylamine NONOate was from Cayman Chemical (Ann Arbor, MI), and other reagents were from Sigma-Aldrich (St. Louis, MO).

**Protein Isolation and Enzymatic Assays.** Wild-type and selenomethione-derivatized apo-HppE was expressed and purified as previously described.[10,15] Apo-protein was concentrated to 30 mg/mL and dialyzed into 0.02 M Tris-HCl, at pH 8.0. Enzyme activity of apo-HppE reconstituted with $Fe(II)(NH_4)_2(SO_4)_2 \cdot 6H_2O$ was determined using a $^{31}P$ NMR assay.[9,10]

**Crystallization of *R*-HPP−Fe(II)−HppE and *R*-HPP−Co(II)−HppE.** *R*-HPP−Fe(II)−HppE crystals were obtained using previous anaerobic conditions for *S*-HPP−Fe(II)−HppE crystals[15] replacing the substrate *S*-HPP with its enantiomer. *R*-HPP (0.6 μL, 0.2 M) was added to Fe(II)−HppE crystals placed over a reservoir of soaking buffer solution (0.1 M HEPES, pH 7.5, 2.5 M ammonium sulfate) and allowed to diffuse into the crystals for 14 h. The crystals were flash-cooled in liquid nitrogen following a 30 s transfer to a cryo-protectant buffer solution (0.1 M Tris-HCl, pH 8.0, 2.0 M ammonium sulfate, 30% (w/v) xylitol).

Crystals of *R*-HPP in complex with Co(II)−HppE were obtained by soaking this substrate into Co(II)−HppE crystals.[15] The hexagonal crystals used for soaking were grown by mixing 2.0 μL of 30 mg/mL selenomethionine−apo-HppE solution in 0.02 M Tris−HCl pH 8.0 with 2.0 μL of precipitant buffer solution (0.1 M Tris−HCl, pH 8.5, 2.0 M ammonium sulfate) using the hanging-drop vapor diffusion method at room temperature. $CoCl_2$ (0.3 μL, 0.1 M) solution was added to the drop, and the so-called "Tris−Co(II)−HppE" crystals grew in 24 h. *R*-HPP−Co(II)−HppE crystals were obtained from Tris−Co(II)−HppE crystals by first transferring crystals to soaking buffer solution to displace any Tris molecules coordinating Co(II). The removal of Tris was verified through a structure determination (data not shown). The Co(II)−HppE crystals were transferred to 4.0 μL of fresh soaking buffer solution for 10 min. *R*-HPP (1.0 μL, 2.5 M) was added to the drop, and the resulting solution was placed over a reservoir of soaking solution for additional 14 h. The crystals were transferred to cryo-protectant buffer solution for 30 s and cooled in liquid nitrogen.

**Crystallization of *S*-HPP−Fe(II)−HppE−NO.** The ternary complex (*S*-HPP−Fe(II)−HppE) was crystallized anaerobically as previously described[15] with slight modifications. *S*-HPP (0.6 μL, 0.2 M) was added to Fe(II)−HppE crystals placed over a reservoir of soaking buffer solution. Nitric oxide (NO) was introduced to the well with *S*-HPP−Fe(II)−HppE crystals by liberation from diethylamine NONOate.[23,24] After 1 h of equilibration, NO gas (2.0 mL) was injected


dx.doi.org/10.1021/ja2025728 |*J. Am. Chem. Soc.* 2011, 133, 11262–11269

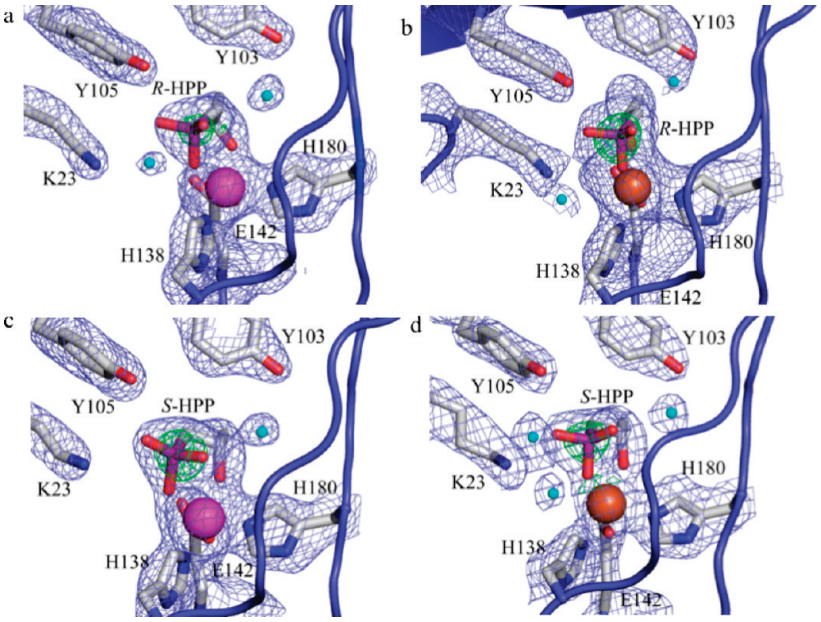


**Figure 2.** Structures of HppE with *R*-HPP or *S*-HPP bound in the active site. (a) Bidentate binding mode for *R*-HPP in the Co(II)−HppE structure. (b) Bidentate binding mode for *R*-HPP in Fe(II)−HppE structure. (c) Bidentate binding mode for *S*-HPP in the Co(II)−HppE structure (1ZZB monomer B). (d) Bidentate binding mode for *S*-HPP in the Fe(II)−HppE structure (1ZZ8 monomer C). Substrate and protein residues are shown as sticks (carbon (gray), oxygen (red), nitrogen (blue), phosphorus (purple)), water molecules as spheres (cyan), Co(II) as a sphere (magenta), and Fe(II) as a sphere (rust). The $2F_o - F_c$ maps (blue mesh) are contoured at 1.0 $\sigma$, and the $F_o - F_c$ omit-maps (green mesh) of the substrate indicating the position of the phosphorus are contoured at 8.0, 10.0, 9.0, and 8.0 $\sigma$, respectively.

into the well for additional 2 h. Crystals were then transferred to cryoprotectant buffer solution and flash-cooled in liquid nitrogen.

**Data Collection and Analysis.** Data sets for *R*-HPP−Fe(II)−HppE and *S*-HPP−Fe(II)−HppE−NO were collected at the Stanford Synchrotron Radiation Lightsource and the Advanced Photon Source, respectively. The *R*-HPP−Co(II)−HppE data set was collected at the Advanced Light Source. The data were integrated and scaled in DENZO and SCALEPACK,[25] respectively (Supporting Information Table 1).

**Structure Determination.** Crystals of *S*-HPP−Fe(II)−HppE−NO ($P4_22_12$; $a,b$ = 111.66 Å, $c$ = 152.16 Å) and *R*-HPP−Fe(II)−HppE ($P4_22_12$; $a,b$ = 111.67 Å, $c$ = 152.81 Å), with three molecules in the asymmetric unit, were isomorphous with our previous crystals of *S*-HPP−Fe(II)−HppE ($P4_22_12$; $a,b$ = 111.65 Å, $c$ = 152.07 Å). Thus, these structures were solved by rigid body refinement in CNS[26] using protein atoms from *S*-HPP−Fe(II)−HppE structure[15] as an initial model (PDB code 1ZZ8). Model building was done in COOT,[27] and iterative refinement steps were accomplished using CNS. Topology and parameter files for *R*-HPP were obtained using HIC-Up.[28] Parameter and topology files for the iron-NO coordination sphere were developed using the bond distances and angles from high-resolution X-ray structures of nonheme iron model complexes with NO bound to iron.[29] To allow movement of atoms away from the average values, weak restraints were used. The CNS protocol included simulated annealing against a maximum likelihood function target, positional refinement, and *B*-factor refinement; noncrystallographic symmetry restraints and sigma cutoff were not used.

Because the *R*-HPP−Co(II)−HppE crystal, consisting of two molecules in the asymmetric unit ($P6_522$; $a,b$ = 86.30 Å, $c$ = 219.1 Å) was isomorphous with our previous crystals of Tris−Co(II)−HppE ($P6_522$; $a,b$ = 86.36 Å, $c$ = 220.17 Å), the *R*-HPP−Co(II)−HppE structure was solved by rigid body refinement in CNS using only protein atoms from the refined Tris−Co(II)−HppE structure[15] as an initial model (PDB code 1ZZC). Iterative model refinement was performed in CNS using the protocol described above. Manual adjustment of the model was performed using XFIT.[30]

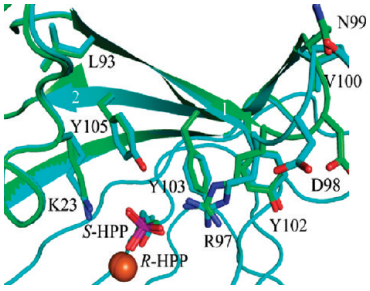


**Figure 3.** Comparison of the cantilever hairpins ($\beta$-strands labeled 1 and 2) of the *R*-HPP−Fe(II)−HppE structure (green) and the *S*-HPP−Fe(II)−HppE structure (cyan). Bound substrate and selected residues are shown as sticks, and iron atoms are shown as spheres (rust).

Structures of *R*-HPP−Co(II)−HppE, *R*-HPP−Fe(II)−HppE, and *S*-HPP−Fe(II)−HppE−NO were analyzed using $2F_o - F_c$ composite omit maps, and Ramachandran geometries were analyzed with PROCHECK.[31,32] The results from PROCHECK indicate that the *R*-HPP−Co(II)−HppE structure has 89.4% of the residues in the most favored and 10.6% of the residues in the additionally allowed regions of the Ramachandran plot. For *R*-HPP−Fe(II)−HppE structure, the Ramachandran plot indicates that 87.7% of the residues are in the most favored and 12.3% of the residues are in the additionally allowed regions. The Ramachandran plot for *S*-HPP−Fe(II)−HppE−NO structure indicates that 86.2% of the residues are in the most favored, 13.6% of the residues are in the additionally allowed regions, and 0.2% of the residues in the generously allowed regions. Chain A of the *R*-HPP−Co(II)−HppE structure contains residues 5−198, while other chains consist of residues 6−198.

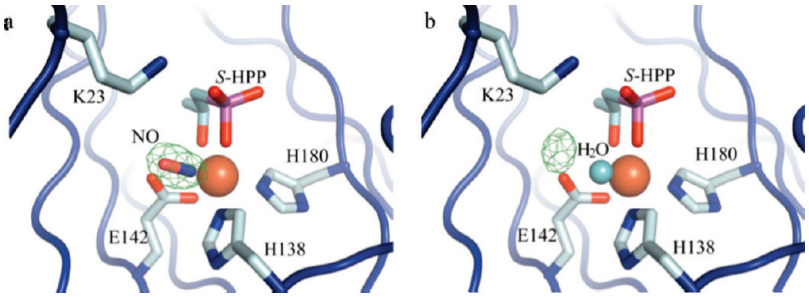


**Figure 4.** The structure of *S*-HPP−Fe(II)−HppE in complex with NO. (a) The active site of *S*-HPP−Fe(II)−HppE is shown with the Fe(II) atom (rust) as a sphere and substrate, residues, and NO as sticks. An $F_o - F_c$ omit map (green mesh) is contoured at 7.0 $\sigma$. (b) When water is refined in a position similar to that of the nitrogen of NO in the active site, shown in Figure 4a, positive $F_o - F_c$ difference density (green mesh) at 4.0 $\sigma$ indicates that water is not large enough to account for the density.

## RESULTS

**Structures of HppE with *R*-HPP.** The crystal structure of Co(II)−HppE in complex with *R*-HPP was solved to 2.1 Å resolution (Figure 2a, Supporting Information Table 1). *R*-HPP−Co(II)−HppE is catalytically inert under aerobic conditions[9] and allows us to observe at high resolution an enzyme state that mimics the form of the enzyme prior to dioxygen binding. We have also solved this same structure using the native Fe(II) metal ion in the absence of dioxygen (Figure 2b), but to lower resolution (3.0 Å). We find that the overall structures are similar, with root-mean-square deviations of 0.27−0.71 Å. In each case, substrate can be unambiguously positioned in the active site due to the presence of 8−10 $\sigma$ electron density peaks that identify the position of the HPP phosphorus atom (Figure 2). As was the case for the *S*-enantiomer, *R*-HPP binds to the active site metal in a bidentate binding mode coordinated by both the C2 hydroxyl and the C1 phosphonate moieties (Figure 2a−d; also see Supporting Information Figure 1a−1e).[15] The bidentate binding mode is observed in both the Fe(II) and the Co(II) structures (see Supporting Information Table 2 for a complete list of structures).

**Conformational Change Closing Active Site.** HppE appears to use an induced-fit mechanism to protect high-energy iron−oxygen species formed during catalysis.[15] A $\beta$-hairpin called the cantilever hairpin (residues 90−107) responds to the physiological substrate *S*-HPP when bound to the enzyme in the correct orientation by moving in and sealing off the top portion of the active site, leaving only a small opening for dioxygen to enter.[15] Comparison of *S*-HPP−Fe(II)−HppE structures with the alternative *R*-HPP substrate shows a similar response; the cantilever hairpin closes down and becomes more ordered upon bidentate substrate binding. In fact, in the closed conformation, the cantilever hairpin in the *R*-HPP−Fe(II)−HppE structure superimposes well with that in the *S*-HPP−Fe(II)−HppE structure (PDB ID 1ZZ8) (Figure 3), producing very similar interactions between the protein and *S*- and *R*-HPP substrates.

A number of hydrogen bonds and electrostatic interactions made by the protein with the substrate are contributed from residues of the cantilever hairpin (Arg97 and Tyr105). Other contacts are made from other $\beta$-barrel residues as well as one residue of the helical domain (Lys23). In the bidentate conformation of both *S*- and *R*-HPP, all hydrogen-bonding interactions are made to the phosphonate moiety. In every structure, the phosphonate substituent is stabilized by charge−charge interactions with Lys23 from the helical domain and hydrogen-bonding interactions with Tyr105 and Asn135 of the $\beta$-barrel (Supporting Information Figure 1). In the majority of both the *S*-HPP and the *R*-HPP bound Fe-HppE structures, Arg97 is ordered and contacts the phosphonate moiety both directly and indirectly via a water molecule to further stabilize the additional charge in the active site (Supporting Information Figure 1c−i).

**Structure with NO as Mimic for Dioxygen Binding.** With the hairpin closed, there is space available for oxygen to enter the active site in a cavity created at the interface of the helical and $\beta$-barrel domains.[15] This cavity leads to the only open coordination site in any of the substrate-bound structures, a position trans to His180. To obtain experimental evidence that this site is in fact the oxygen binding site, NO was used as an $O_2$ mimic. Similar to previously observed structures of *S*-HPP−Fe(II)−HppE,[15] the structure of *S*-HPP−Fe(II)−HppE−NO at 2.85 Å resolution reveals bidentate coordination of the substrate to the Fe(II) center via the C2 hydroxyl and the phosphonate oxygen in all three molecules in the asymmetric unit. In one of the three monomers, there is density only for a water molecule and not for NO (Supporting Information Figure 1h). However, in the other two monomers (monomers A,B (Fe−*S*-HPP−NO)), NO is coordinated to the Fe(II) center as seen by omit and positive difference electron density that is consistent with a diatomic molecule (Figure 4a,b; also see Supporting Information Figure 1f,g). When a water molecule is refined into the electron density of monomers A and B instead of NO, positive difference electron density results, indicating the presence of a second atom (Figure 4b). When NO is refined in this position, no positive or negative difference electron density appears, indicating that a diatomic molecule is the correct size.

Because the only difference between the *S*-HPP−Fe(II)−NO structure and the previous *S*-HPP bound Fe−HppE structures is the soaking of the crystals with NO, we have modeled and refined NO in this site in these two monomers. We find that, as predicted, NO coordinates trans to the His180 iron ligand, presumably via the nitrogen atom in the site that was "open" in the substrate-bound structure. The Fe−N bond distances in the two NO bound monomers are 1.64 and 1.66 Å, and the Fe−N−O bond angles are 160° and 161°, which are typical values for iron−nitrosyl interactions in model complexes.[29] The oxygen atom of the NO is pointed toward C1 of the substrate at an average distance of 3.5 Å. C1 is the proposed carbon from which a hydrogen atom is abstracted.[9] While it was predicted previously that Lys23 could interact with the active oxygen

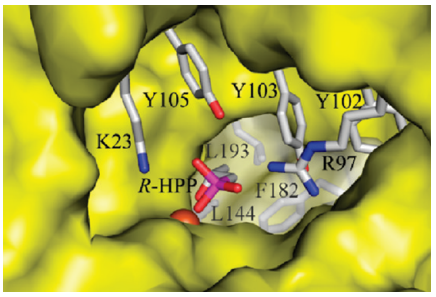


**Figure 5.** Substrate binding pocket. Cantilever hairpin residues and residues interacting with the aliphatic portion of *R*-HPP (L144, L193, and F182) are shown as sticks. Iron is shown as a sphere (rust).

species,[15] here we find that the oxygen atom of NO is far from the terminal amine of Lys23 (~4.8 Å in monomer A and ~5.2 Å in the monomer B), although movement of this residue is possible. Alternatively, Lys23 may play its essential role[15] at some other stage in the mechanism.

**Water Binding Site Trans to His180.** Many of the HppE structures that have bound substrate also have highly ordered water molecules in the active site. Of particular interest are water molecules, which are found in the *R*-HPP−HppE structures and lie near Lys23 in a position trans to facial triad ligand His180 without coordinating the metal (Figure 2a,b). A water molecule was observed in a similar position in one of three active sites within the asymmetric unit of the previously determined *S*-HPP−Fe(II)−HppE structure in tetragonal space group[15] (Figure 2d). There is a range of distances that waters can occupy in this general water binding region (2.5−3.9 Å). Waters located at approximately 2.8 Å from the metal are in the same position as the terminal oxygen of NO when it is bound in the open metal coordination site (comparable to the second oxygen of dioxygen) (Figure 2b,d; also see Supporting Information Figure 1e,i). Waters at distances of ~3.9 Å from the metal may represent a product water position (Figures 2a; also see Supporting Information Figure 1a,b).

**Comparison of Bidentate *R*- and *S*-HPP Binding.** With experimental information from our NO data supporting the assignment of the binding site for dioxygen on iron, we can examine the proposed mechanisms for regiospecificity by comparing our *S*-HPP and *R*-HPP bound structures. Both enantiomers bind to the same general site on the metal in the active site of HppE. For *S*-HPP, its hydrophobic portion including the C2 methyl group is accommodated by a hydrophobic pocket on the enzyme, comprising residues Phe182, Leu193, and Leu144 (Figure 5).[15] Because the position of the C2 methyl moiety of the *R*-HPP molecule (bidentate binding mode) is within 1 Å of the corresponding position of the C2 methyl moiety of *S*-HPP (Figure 6a), the same hydrophobic binding pocket serves to accommodate the methyl moiety of the *R*-enantiomer (Figure 5).

Even though the binding modes for both substrate enantiomers are similar, they are not identical (Figure 6a), and even small differences in orientations of C1 and C2 can have a significant impact in terms of accessibility of their hydrogens for abstraction by the reactive iron−oxygen intermediates. While hydrogen atoms are not discernible in electron density, the orientation of the $sp^3$ carbon atoms (i.e., tetrahedral carbon atoms) can be accurately modeled within the electron density. Therefore, the positions of the hydrogen atoms covalently bound to these carbon atoms can be inferred. Using the binding site of

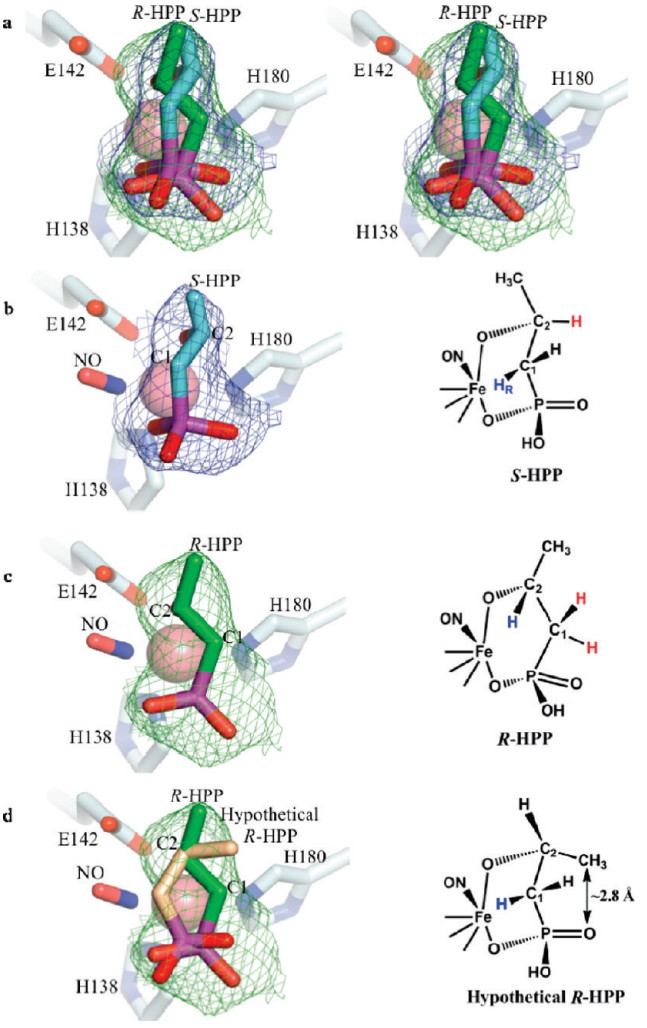


**Figure 6.** Structural insights into HppE regiospecificity. (a) Stereoview comparing a $2F_o - F_c$ omit map density (contoured at 1.0 $\sigma$) of *S*-HPP (cyan carbons, blue mesh) and *R*-HPP (green carbons, green mesh) from the Co(II)−HppE structures. (b) $2F_o - F_c$ omit map density (left) and cartoon (right) for *S*-HPP, with accessible hydrogen atom in blue and inaccessible hydrogens in red. (c) $2F_o - F_c$ omit map density (left) and cartoon (right) for *R*-HPP. Hydrogen atoms labeled as in (b). (d) Left, superposition of *R*-HPP (carbons in green) with a hypothetical conformation (not observed) of *R*-HPP (carbons in wheat) in omit map density for *R*-HPP. Right, chemical structure of *R*-HPP shown in a hypothetical conformation (not observed) shown as in (d), left. Accessible hydrogen in blue, and arrow indicates predicted distance. Position of NO from the NO−*S*-HPP−Fe(II)−HppE structure is shown in (b)−(d) for reference.

NO to mark the likely location of the dioxygen binding site, the modeling of hydrogens suggests that for the *S*-HPP substrate, the Pro-R hydrogen at C1 points toward this putative dioxygen binding site (3.5 Å between O of NO and C1), while the C2 hydrogen is oriented in the opposite direction (4.3 Å between O of NO and C2) (Figure 6b). In contrast, for the *R*-HPP structures, the modeled C1 methylene hydrogens point away from (4.0 Å between O of NO and C1) while the C2 hydrogen points toward the dioxygen binding site (3.1 Å between O of NO and C2) (Figure 6c). Thus, despite the similar bidentate binding modes, the orientation of the C1 and C2 carbons and their hydrogen atoms appear to be quite different.

**Scheme 2. Proposed Mechanisms for the Oxidation of *S*- and *R*-HPP by HppE[a]**

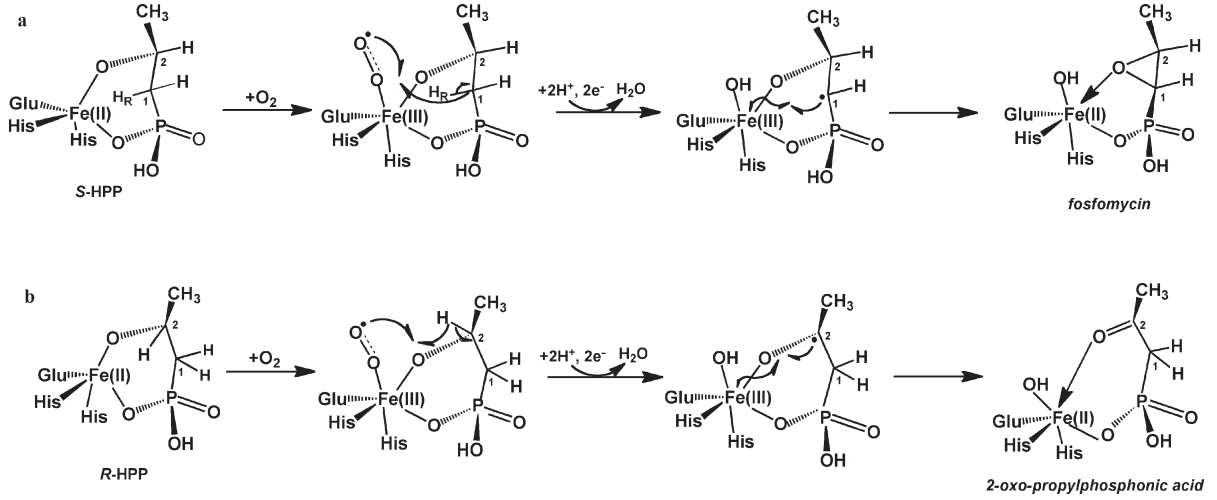


[a] (a) Conversion of *S*-HPP to fosfomycin is initiated by H-atom abstraction from C1. (b) Conversion of *R*-HPP to the keto-product probably occurs via H-atom abstraction from C2.

It is interesting to consider why *R*-HPP binds to the iron with such a difference in the positions of C1 and C2 as compared to *S*-HPP, and whether at this resolution we can be sure of this alternative conformation. When we compare the refined model of *R*-HPP (green in Figure 6c,d) with a hypothetical conformation of *R*-HPP that is based on the *S*-substrate conformation (wheat in Figure 6d), we find that there is no electron density to support the placement of the methyl group on C2 in the conformation represented by the hypothetic model (Figure 6d). The alternative conformation is a much better fit to the density. In considering why the hypothetical conformation is not favored, modeling suggests that the methyl group on C2 would be close (2.8 Å) to the phosphonic acid moiety in this conformation, producing a steric clash (Figure 6d). The electron density is consistent with an extended and staggered conformation of *R*-HPP in which the methyl moiety is farthest from the bulky phosphonic acid moiety (Figure 6c; also see Supporting Information Figure 2).

## DISCUSSION

Mononuclear iron enzymes catalyze a wide range of reactions from antibiotic biosynthesis to DNA repair. While the products of the reactions vary, most mononuclear iron enzymes must accomplish the same tasks (activate the iron center to facilitate dioxygen binding, protect high energy intermediates throughout the catalytic cycle, and reduce dioxygen).[9,10,12,15,21,33] Our goal with these structural analyses is to address the directing factors by which HppE converts each substrate to its final product, providing insight into the mechanisms of regiospecificity.

For the mechanism of the enzyme with its natural substrate, *S*-HPP, much is already known, and here we provide structural insight into dioxygen binding. For *R*-HPP, no structural data were available, and we wished to obtain crystallographic snapshots for the stages of catalysis and compare these results to those for *S*-HPP. First, in considering how the Fe(II/III) potential is modulated in HppE to favor oxidation by dioxygen, our previous snapshots of *S*-HPP−HppE suggested that direct bidentate binding of the electron-donating substrate molecule *S*-HPP to Fe(II) would be sufficient to activate the iron center.[15] We now observe that *R*-HPP also binds to iron in a bidentate manner via its phosphonate and hydroxyl oxygen atoms (Figure 2). Second, we previously considered how reactive intermediates are protected in the HppE active site when *S*-HPP is the substrate. We identified an induced fit mechanism in which a switch in the *S*-HPP binding mode from monodentate to bidentate induces a conformational change of two $\beta$-strands that seals off part of the active site, protecting reactive catalytic intermediates.[15] Interestingly, this induced fit mechanism is in play with *R*-HPP as well (Figure 3). Because the two enantiomeric substrates use the same coordination sites for binding to iron and both use the same binding pocket in the enzyme (Figures 2 and 5), both substrates are able to induce the same conformational change in the $\beta$-hairpin upon bidentate substrate binding.

While much of the active site is buried from solvent due to this conformational change, there is a small channel available for dioxygen to enter and reach the only open coordination site on Fe in the *S*-HPP bound HppE structures.[15] We have proposed that this site is the location of dioxygen binding.[15] Here, we use NO as a mimic for dioxygen binding and confirm that NO does bind to this open coordination site (Figure 4), providing the first structural evidence in support of this hypothesis. The binding of dioxygen to the Fe(II) center is proposed to lead to the reversible formation of a transient Fe(III)−superoxo species[9,21] and facilitate hydrogen atom abstraction from *S*-HPP (Scheme 2a).[20,34] In the final steps of the mechanism, the substrate radical intermediate collapses, forming the epoxide product fosfomycin, while dioxygen is fully reduced in the presence of NAD(P)H, forming two water molecules (Scheme 2a). One water molecule may remain bound to iron until it is displaced by the binding of a second substrate molecule, consistent with the observation of multiple water molecules bound to iron in the absence of substrate.[15] The second water molecule would be released from iron and may occupy the farther water binding site (3.9 Å), trans to His180 as described above.

While this series of structures nicely explains the observed reaction of *S*-HPP with HppE to form an epoxide, so far this discussion has only noted similarities between *S*-HPP and *R*-HPP binding and has not described any differences that can

be invoked to explain why *R*-HPP forms a ketone rather than an epoxide product. Our structural data suggest that the formation of different products is not due to the use of differential binding sites on the enzyme, but rather it is due to the conformation that the substrate itself must assume such that it fits well into the same binding site in the enzyme. For *R*-HPP to bind in a bidentate mode to Fe, utilizing the same binding pocket on the enzyme, adjustments must be made, but here it is the substrate rather than the enzyme that adjusts. *R*-HPP adopts an extended and staggered conformation that places the phosphonate moiety as far as possible from the methyl group (Figure 6, also see Supporting Information Figure 2). The result of this conformational difference is that the C2 hydrogen is now closer to the dioxygen binding site than either C1 hydrogen, providing a structural rather than a chemical rationale for the observed regiospecificity in HppE catalysis. These findings are consistent with the fluoride analogue data,[22] which suggest that abstraction of a C1 hydrogen is involved in epoxide formation from *S*-HPP, but not in ketone formation from *R*-HPP (Scheme 1). For *S*-HPP, abstraction of the C1 *pro-R* hydrogen by the iron−superoxo intermediate (Scheme 2a) would yield a substrate radical centered at C1, which could collapse into the epoxide product. For *R*-HPP, hydrogen atom abstraction from C2 would lead to a C2-centered radical intermediate, which could collapse into the ketone product, 2-oxo-propylphosphonic acid (Scheme 2b).

## CONCLUSIONS

This series of structures has allowed us to probe the mechanism of regiospecificity for HppE, a fascinating variant in the nonheme mononuclear iron family of enzymes. We now have structural evidence for the manner in which both the *S*- and the *R*-enantiomers of the substrate bind, as well as for the location of dioxygen binding to Fe. This first three-dimensional visualization of enantiomeric substrate recognition provides new insight into the stereospecificity afforded by a mononuclear nonheme iron enzyme.

## ASSOCIATED CONTENT

**Supporting Information.** Two-dimensional active site contact maps (Figure 1a−i), Newman projections of substrates bound to iron (Figure 2), data collection and refinement statistics table (Table 1), and structures in paper table (Table 2). This material is available free of charge via the Internet at http://pubs.acs.org. The structures are deposited in the Protein Data Bank with PDB entries 3SCF, 3SCG, and 3SCH.

## AUTHOR INFORMATION

### Corresponding Author

cdrennan@mit.edu

### Present Addresses

[⊥]Harbor Hospital, 3001 South Hanover Street, Baltimore, Maryland 21225, United States.

## ACKNOWLEDGMENT

This work was supported in part by National Institutes of Health Grants GM40541 (HWL), F32 GM079966 (DY), and Center Grant P30 ES002109. C.L.D. is a Howard Hughes Medical Institute Investigator. Data were collected at the Advanced Light Source (ALS), Stanford Synchrotron Radiation Laboratory (SSRL), and the Advanced Photon Source (APS). Support for the synchrotron sources is provided by the U.S. Department of Energy (ALS, SSRL, and APS) and by the National Institutes of Health (SSRL).

## REFERENCES

(1) Lobel, B. *Int. J. Antimicrob. Agents* **2003**, *22*, 85–87.
(2) Nakazawa, H.; Kikuchi, Y.; Honda, T.; Isago, T.; Nozaki, M. *J. Infect. Chemother.* **2003**, *9*, 304–309.
(3) Cassone, M.; Campanile, F.; Pantosti, A.; Venditti, M.; Stefani, S. *Microb. Drug Resist.* **2004**, *10*, 43–49.
(4) Brown, E. D.; Marquardt, J. L.; Lee, J. P.; Walsh, C. T.; Anderson, K. S. *Biochemistry* **1994**, *33*, 10638–10645.
(5) Marquardt, J. L.; Brown, E. D.; Lane, W. S.; Haley, T. M.; Ichikawa, Y.; Wong, C.-H.; Walsh, C. T. *Biochemistry* **1994**, *33*, 10646–10651.
(6) Munos, J. W.; Moon, S.-J.; Mansoorabadi, S. O.; Chang, W.; Hong, L.; Yan, F.; Liu, A.; Liu, H. W. *Biochemistry* **2008**, *47*, 8726–8735.
(7) Liu, P.; Mehn, M. P.; Yan, F.; Zhao, Z.; Que, L.; Liu, H. W. *J. Am. Chem. Soc.* **2004**, *126*, 10306–10312.
(8) Hammerschmidt, F.; Kaehlig, H. *J. Org. Chem.* **1991**, *56*, 2364–2370.
(9) Liu, P.; Liu, A.; Yan, F.; Wolfe, M. D.; Lipscomb, J. D.; Liu, H. W. *Biochemistry* **2003**, *42*, 11577–11586.
(10) Liu, P.; Murakami, K.; Seki, T.; He, X.; Yeung, S.-M.; Kuzuyama, T.; Seto, H.; Liu, H. W. *J. Am. Chem. Soc.* **2001**, *123*, 4619–4620.
(11) McLuskey, K.; Cameron, S.; Hammerschmidt, F.; Hunter, W. N. *Proc. Natl. Acad. Sci. U.S.A.* **2005**, *102*, 14221–14226.
(12) Yan, F.; Munos, J. W.; Liu, P.; Liu, H. W. *Biochemistry* **2006**, *45*, 11473–11481.
(13) Dunwell, J. M.; Purvis, A.; Khuri, S. *Phytochemistry* **2004**, *65*, 7–17.
(14) Yan, F.; Li, T.; Lipscomb, J. D.; Liu, A.; Liu, H. W. *Arch. Biochem. Biophys.* **2005**, *442*, 82–91.
(15) Higgins, L. J.; Yan, F.; Liu, P.; Liu, H. W.; Drennan, C. L. *Nature* **2005**, *437*, 838–844.
(16) Cicchillo, R. M.; Zhang, H.; Blodgett, J. A.; Whitteck, J. T.; Li, G.; Nair, S. K.; van der Donk, W. A.; Metcalf, W. W. *Nature* **2009**, *459*, 871–875.
(17) Zhou, J.; Kelly, W. L.; Bachmann, B. O.; Gunsior, M.; Townsend, C. A.; Solomon, E. I. *J. Am. Chem. Soc.* **2001**, *123*, 7388–7398.
(18) O'Brien, J. R.; Schuller, D. J.; Yang, V. S.; Dillard, B. D.; Lanzilotta, W. N. *Biochemistry* **2003**, *42*, 5547–5554.
(19) Matthews, M. L.; Krest, C. M.; Barr, E. W.; Vaillancourt, F. H.; Walsh, C. T.; Green, M. T.; Krebs, C.; Bollinger, J. M. *Biochemistry* **2009**, *48*, 4331–4343.
(20) Bollinger, J. M.; Krebs, C. *Curr. Opin. Chem. Biol.* **2007**, *11*, 151–158.
(21) Mirica, L. M.; McCusker, K. P.; Munos, J. W.; Liu, H. W.; Klinman, J. P. *J. Am. Chem. Soc.* **2008**, *130*, 8122–8123.
(22) Zhao, Z.; Liu, P.; Murakami, K.; Kuzuyama, T.; Seto, H.; Liu, H. W. *Angew. Chem., Int. Ed.* **2002**, *41*, 4529–4532.
(23) Keefer, L. K.; Nims, R. W.; Davies, K. M.; Wink, D. A. *Methods Enzymol.* **1996**, *268*, 281–293.
(24) Maragos, C. M.; Morley, D.; Wink, D. A.; Dunams, T. M.; Saavedra, J. E.; Hoffman, A.; Bove, A. A.; Isaac, L.; Hrabie, J. A.; Keefer, L. K. *J. Med. Chem.* **1991**, *34*, 3242–3247.
(25) Otwinowski, Z.; Minor, W. *Methods Enzymol.* **1997**, *276*, 307 326.
(26) Brünger, A. T.; Adams, P. D.; Clore, G. M.; DeLano, W. L.; Gros, P.; Grosse-Kunstleve, R. W.; Jiang, J.-S.; Kuszewski, J.; Nilges, M.; Pannu, N. S.; Read, R. J.; Rice, L. M.; Simonson, T.; Warren, G. L. *Acta Crystallogr.* **1998**, *D54*, 905–921.
(27) Emsley, P.; Cowtan, K. *Acta Crystallogr.* **2004**, *D60*, 2126–2132.
(28) Kleywegt, G. J.; Jones, T. A. *Acta Crystallogr.* **1998**, *D54*, 1119 1131.

(29) Chiou, Y.-M.; Que, L. *Inorg. Chem.* **1995**, *34*, 3270–3278.
(30) McRee, D. E. *J. Struct. Biol.* **1999**, *125*, 156–165.
(31) Ramachandran, G. N.; Ramakrishnan, C.; Sasisekharan, V. *J. Mol. Biol.* **1963**, *7*, 95–99.
(32) Laskowski, R. A.; MacArthur, M. W.; Moss, D. S.; Thornton, J. M. *J. Appl. Crystallogr.* **1993**, *26*, 283–291.
(33) Whitteck, J. T.; Malova, P.; Peck, S. C.; Cicchillo, R. M.; Hammerschmidt, F.; van der Donk, W. A. *J. Am. Chem. Soc.* **2011**, *133*, 4236–4239.
(34) Costas, M.; Mehn, M. P.; Jensen, M. P.; Que, L. *Chem. Rev.* **2004**, *104*, 939–986.